Solar Energy, Vol. 23, pp. 497–507
Pergamon Press Ltd., 1979. Printed in Great Britain

SHADOW EFFECT OF ADJACENT SOLAR COLLECTORS IN LARGE SCALE SYSTEMS

J. APPELBAUM and J. BANY
Tel-Aviv University, School of Engineering, Tel-Aviv, Israel

(*Received* 18 *September* 1978; *revision accepted* 15 *June* 1979)

Abstract—In large scale solar systems and in other cases with limited field area (such as on tops of buildings), shadowing of collectors, (thermal or photovoltaic) by their neighbours might occur during the day. This situation calls for an optimal solution of collector deployment in a given field area for maximum or desired energy.

The paper deals firstly with the shadowing analysis of vertical and inclined poles and collectors (the shadow components, height and area). This useful information is used in an example of optimal deployment of collectors in a given area (which includes the tilt angle, collector size, spacing between collectors and the number of collector rows).

INTRODUCTION

The design of large scale solar plants (thermal or photovoltaic) of different kinds is increasing and shading of collectors by their neighbours may become unavoidable. The question of "real estate" for the installation of the collectors may appear to be acute as in limited area such as on tops of buildings. In these cases where maximum or required collected energy is desired, the collectors that are arranged in rows are shaded during the day.

The trivial solution of a single collector tilted at its optimum angle is not practical for many technical reasons, or sometimes, the permitted added height of the collector is limited. Therefore, the collectors are arranged in many rows with some spacing for maintenance purposes. In this arrangement[1], collectors of one row can cause shadow on the adjacent row during the day, thus decreasing the amount of collected energy. The shading effect depends on the spacing between collectors, their height, the row length, the tilt angle and the latitude. Many rows will on one hand increase the gross collector area (small spacing) but on the other hand, also increase the shading effect. There is, therefore, an optimal solution for the deployment of the collectors in a given field area from the collected energy as well as from an economical point of view.

The purpose of this paper is to calculate the shading effect of vertical and inclined poles and collectors and its significance to the design of the field of collectors. Analytical expressions of the shadow's east and west components (for a south faced collector), shadow height and area were derived. Figures show the shading effect for different months and collector spacings. An estimation of the collector spacing for different latitudes was made. A detailed example is given that shows the recommended (optimal) deployment of the collectors in a given field area.

SHADOW OF A VERTICAL POLE

Figure 1 shows the shadow components of a pole of height H at the origin. The sun is in altitude α (at solar hour angle ω) and in azimuth γ. The shadow length F is

$$F = H/\tan\alpha. \tag{1}$$

The relation between the sun altitude α, latitude ϕ, declination angle δ and the hour angle ω, is given by[2]

$$\sin\alpha = \sin\phi\sin\delta + \cos\phi\cos\delta\cos\omega. \tag{2}$$

The east–west shadow component is

$$F_x = H\frac{\sin\gamma}{\tan\alpha}. \tag{3}$$

It can be shown ([2], p. 34 and after some manipulations)

$$F_x = H\frac{\cos\delta\sin\omega}{\sin\phi\sin\delta + \cos\phi\cos\delta\cos\omega} \tag{4}$$

similarly, the north–south component is

$$F_y = H\frac{\cos\gamma}{\tan\alpha} \tag{5}$$

and it can be shown ([2] p. 34) that

$$F_y = H\frac{\sin\phi\cos\delta\cos\omega - \cos\phi\sin\delta}{\sin\phi\sin\delta + \cos\phi\cos\delta\cos\omega}. \tag{6}$$

Equations (4) and (6) give the pole shadow components as a function of time (the solar hour angle ω—the hour during the day, and the declination angle δ—the date in the year) and the location (the latitude ϕ). The relation between the solar time τ and the hour angle ω is given by

$$\tau = \left(\frac{180+\omega}{360}\right)24$$

or

$$\omega = 180 - 15\tau. \tag{7}$$

Figures 2 and 3 shows the shadow components F_y/H and F_x/H, respectively, calculated according to the eqns (4), (6) and (7) for Tel-Aviv area (latitude $\phi = 32°00'$N) of a pole at the origin O for some typical months. The declination angle values are given in Table 1[3]. The

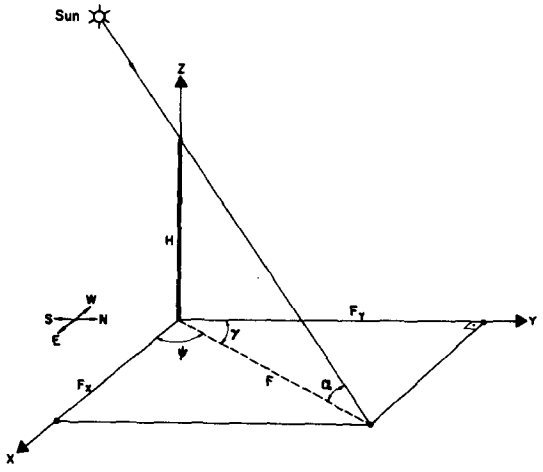

Fig. 1. Shadow components of a vertical pole.

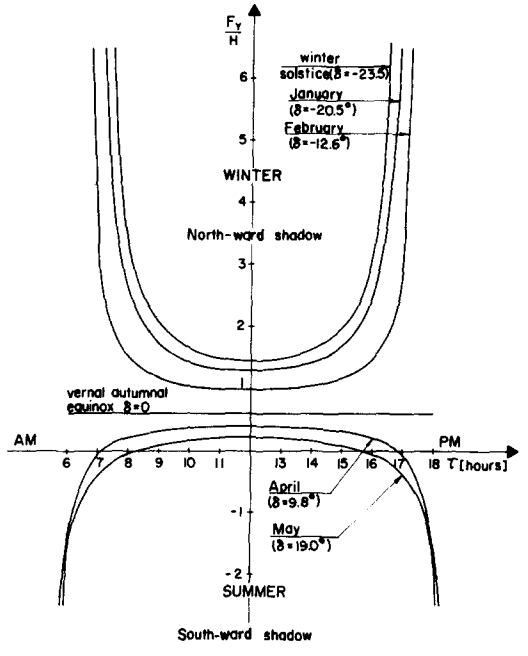

Fig. 2. North–South shadow components of a vertical pole as a function of time.

shadows are shown for the winter months January ($\delta = -20.5°$) and February ($\delta = -12.6°$) and the winter solstice day, and for the summer months April ($\delta = 9.8°$), May ($\delta = 19.0°$) and for the vernal and autumnal equinox

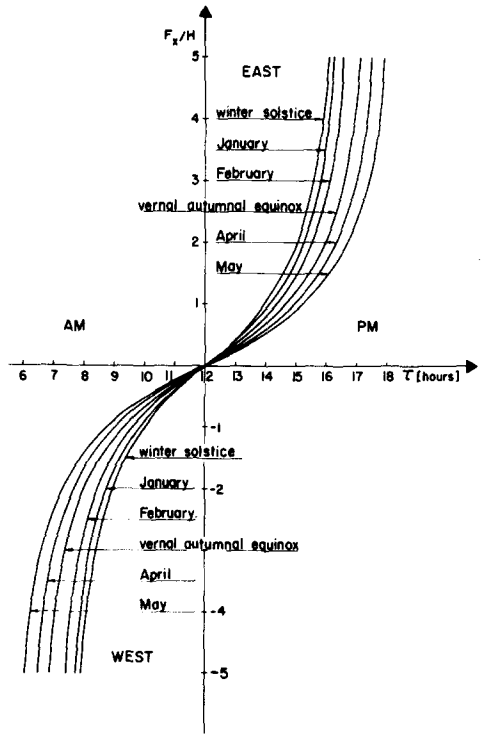

Fig. 3. East–West shadow components of a vertical pole as a function of time.

days, $\delta = 0°$. The sunrise ($-\omega_{ss}$) and sunset ω_{ss}) hour angles were obtained by setting $\alpha = 0$ in eqn (2)

$$\cos \omega_{ss} = -\tan \phi \tan \delta \tag{8}$$

At winter time, Fig. 2, the shadows are long and in the northern direction. At noon, the shadow is short and increases to infinity toward the sun rise and set times. The longest shadows are for the winter solstice day and the minimal value at noon is $F_y/H = 1.45$. At summer time ($\delta > 0$), the shadows are short and most of the day they are in the northward direction. At sunrise and sunset periods, for which $90° < \gamma < -90°$ the shadows are in the southward direction. For April, at $\tau = 07{:}06$ and $\tau = 16{:}54$, $|\gamma| = 90°$ and the shadows are exactly at west and east, respectively. A special case happens at the vernal and autumnal equinox ($\delta = 0$). The north–south shadow component is constant during the day and is $F_y/H = 0.62$. The southward shadows in summer are of minor importance since the isolation at these times is low

Table 1. Average values of declination angle

Month	Jan.	Feb.	21 Mar.	Mar.	Apr.	May	June	21 June
$\delta°$	−20.5	−12.6	0	0.2	9.8	19.0	23.1	23.45

Month	July	Aug.	Sept.	21 Sept.	Oct.	Nov.	Dec.	21 Dec.
δ^0	20.7	12.6	1.4	0	−10.2	−19.2	−23.1	−23.45

and collectors are faced to the south. Figure 3 shows the east–west shadow components for the same months as in Fig. 2.

Figure. 4 describes the relation between the shadow components $F_y = f(F_x)$ for the months as in the preceeding figures, for a pole at the origin. The figure includes the shadow length and direction at different times, 07:30, etc. for February, shown by the rays. The shadow angle with the east-west direction is obtained from eqns (4) and (6)

$$\tan\psi = \frac{F_y}{F_x} = \frac{\sin\phi\cos\delta\cos\omega - \cos\phi\sin\delta}{\cos\delta\sin\omega} \tag{9}$$

This angle has a limit for $\omega = \omega_{ss}$, and by using eqn (8) the limit is

$$\psi_{ss} = \arctan\left(1\Big/\sqrt{\frac{\cos^2\phi}{\tan^2\delta} - \sin^2\phi}\right) \tag{10}$$

which is 14.89° for February (dashed lines). The F_y, F_x plane is divided into two regions, the shaded ABCDOE and the unshaded regions. Similar regions are obtained for different months. *Any second pole in the ABCDOE region will be shaded once during the day.*

For the vernal and autumnal equinox days, the sun rises exactly in the east ($\gamma = -90°$). In winter ($\delta < 0$), the sun rises at south-east direction $|\gamma| < 90°$, therefore the shadow points to north–west. In summer ($\delta > 0$) the sun rises in the north-east $|\gamma| > 90°$ and the shadow points to south–west.

SHADOW OF A VERTICAL COLLECTOR

A wall (collector) can be considered as composed of an infinite number of poles. A collector of length $OL = L/H = 7.5$ and its shadow are shown in Fig. 5. The 2 curves E and F (heavy lines) correspond to the collector edges O and L shadows, for January. The collector shadows for the times $\tau = 07{:}30$ (left) and $\tau = 16{:}30$ (right) are shown by the dashed areas. At 07:30, the O edge causes the OR shadow, and the L edge causes the LP shadow. Hence, the whole collector OL causes the shadow area $ORPL$. Similarly, at 16:30, the collector shadow area is $OQSL$, to the east side.

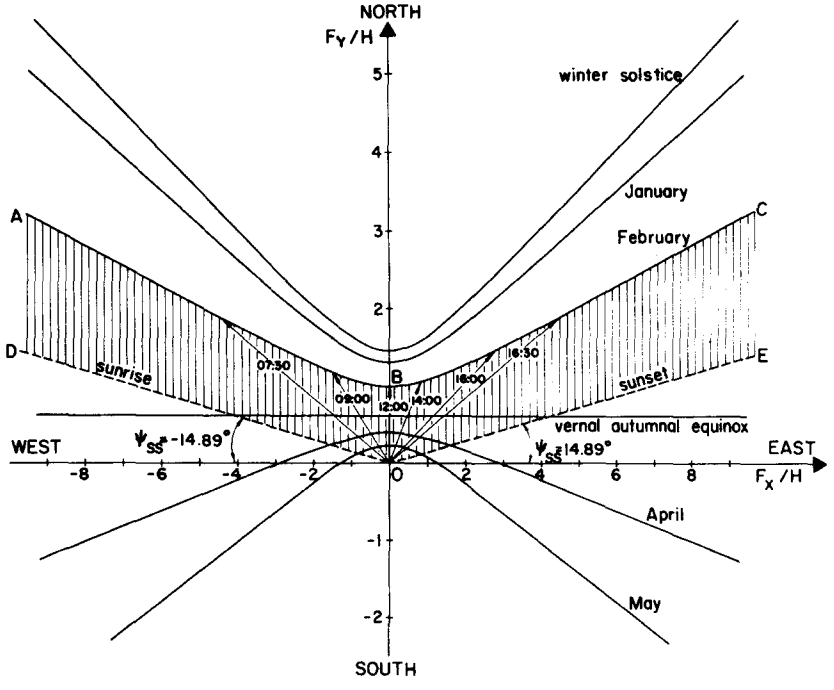

Fig. 4. Shadow variation of a vertical pole.

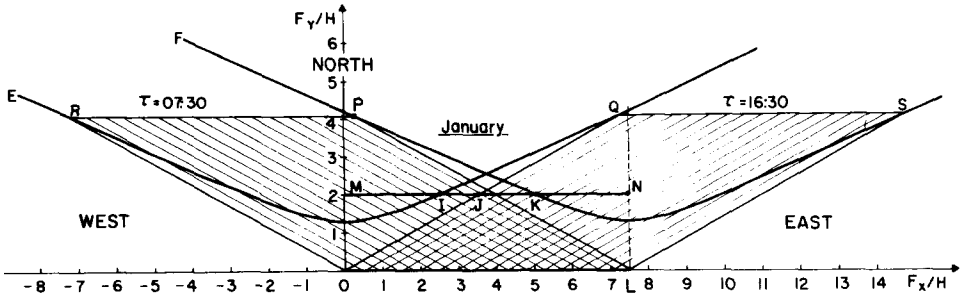

Fig. 5. Shadow of a vertical collector for January.

By placing a second collector MN of the same length and height, at a distance $D/H = 2.0$, the section JN will be shaded at 16:30. The longest shaded part afternoon is $IN = 5.0$ at 15:30, and symetrically, before noon–MK = 5.0 at 08:30. The collector MN is unshaded from time 08:30 to 15:30, since the shadow component F_y/H is less than $D/H = 2$ during that time.

SHADOW OF AN INCLINED POLE

A pole of length A, in the ZY plane, inclined northward at an angle β, is depicted in Fig. 6. The shadow length is $P = \overline{OC}$ and the components are

$$P_x = A \sin\beta \frac{\sin\gamma}{\tan\alpha} = F_x \tag{11}$$

$$P_y = A\left(\cos\beta + \frac{\cos\gamma}{\tan\alpha}\sin\beta\right) = A\cos\beta + F_y \tag{12}$$

where F_x and F_y are given in Eqns (4) and (6), and $H = A\sin\beta$. The shadow edge C caused by the inclined pole OO′ at the origin is identical with the shadow edge of a vertical pole $O'R$ of height $H = A\sin\beta$ shifted by $A\cos\beta$. Therefore, Figs. 2, 3 and 4 can be used for an inclined pole with its real height, $A\sin\beta$, and the origin is shifted in the $-y$ direction by $A\cos\beta$.

The shadow angle ψ_{ss} with the east–west direction at time ω_{ss} is

$$\psi_{ss} = \arctan\left(\frac{P_y}{P_x}\right)\Big|_{\omega=\omega_{ss}} = \arctan\left(1\Big/\sqrt{\frac{\cos^2\phi}{\tan^2\delta} - \sin^2\phi}\right) \tag{13}$$

the same result as for a vertical pole.

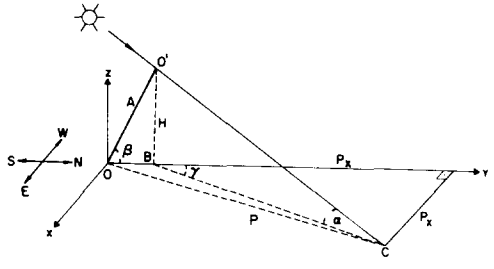

Fig. 6. Shadow components of an inclined pole.

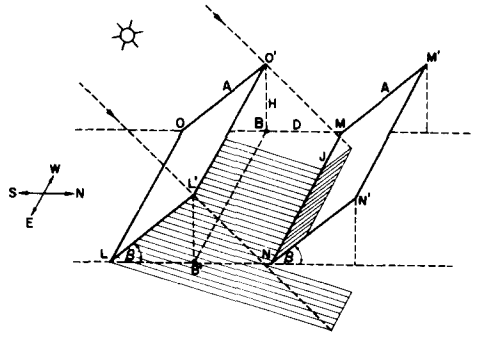

Fig. 7. Position of two inclined collectors.

SHADOW OF AN INCLINED COLLECTOR

Figure 7 describes the position of two inclined collectors $OLO'L'$ and $MNM'N'$) and the shadow shape caused by the $OLO'L'$ on $MNM'N'$. Figure 8 describes the shadow (shaded area) caused by the inclined collector of Fig. 7 with $\beta = 50°$ for January at $\tau = 16{:}30$. The two curves E and F correspond to the shadows of the collector's two edges OO' and LL' during the day. These curves are identical with the curves in Fig. 5 for a vertical collector $B'BO'L'$ (Fig. 7) of height $O'B = H$ and its basis BB'. Since the inclined collector basis is OL and at a distance $A\cos\beta$ from the line BB' the shadow of the collector edge OO' is OU and not BU as it would be for a vertical collector at B. The distance OB equals $\cot\beta = 0.84$. By placing the collector $MNMN'$ at a distance $BM/H = D/H = 2.0$, the shadow on it is NJ' which is less than for a vertical collector of the same height ($NJ' < NJ$). Therefore, an inclined collector has less shadow effect than a vertical one of the same height. It should be mentioned that part of the shadows are beneath the collector.

SHADOW HEIGHT AND AREA

The calculation of the shadow height and area caused by an inclined collector on another collector is given in Appendix A. The relative shadow height $h = H_s/A$ (in units of collector length A), in the MM' direction (Fig. 7), as a function of time is obtained from eqns (6), (12) and (A 13)

$$h = 1 - \frac{D + A\cos\beta}{P_y} = 1 - \frac{\cos\phi\cos\delta\cos\omega + \sin\phi\sin\delta}{\cos(\phi-\beta)\cos\delta\cos\omega + \sin(\phi-\beta)\sin\delta} \times \frac{D + A\cos\beta}{A} \tag{14}$$

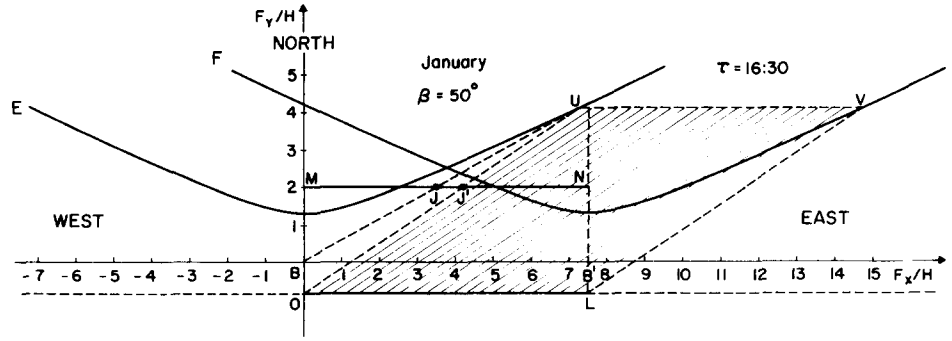

Fig. 8. Shadow of an inclined collector.

where D is the collector spacing ($BM = D$); $h \geq 0$, otherwise $h = 0$.

The relative shaded area, ξ, of an inclined collector is obtained from eqns (4), (6) and (A15)

$$\xi = \left[1 - \frac{\cos\phi\cos\delta\cos\omega + \sin\phi\sin\delta}{\cos(\phi-\beta)\cos\delta\cos\omega + \sin(\phi-\beta)\sin\delta} \times \frac{D + A\cos\beta}{A}\right] \times \left[1 - \frac{\cos\delta\sin\omega\sin\beta}{\cos(\phi-\beta)\cos\delta\cos\omega + \sin(\phi-\beta)\sin\delta} \times \frac{D + A\cos\beta}{L}\right] \quad (15)$$

and $\xi \geq 0$ for non-negative values of both expressions in the parenthesis, otherwise, $\xi = 0$. Defining the relative spacing d and the relative row length l by

$$d = D/H, \quad l = L/H \quad (16)$$

(where $H = A\sin\beta$) and substituting in eqns (14) and (15), we obtain

$$h = 1 - \frac{\cos\phi\cos\delta\cos\omega + \sin\phi\sin\delta}{\cos(\phi-\beta)\cos\delta\cos\omega + \sin(\phi-\beta)\sin\delta} \times (d\sin\beta + \cos\beta) \quad (17)$$

and $h \geq 0$, otherwise $h = 0$.

$$\xi = \left[1 - \frac{\cos\phi\cos\delta\cos\omega + \sin\phi\sin\delta}{\cos(\phi-\beta)\cos\delta\cos\omega + \sin(\phi-\beta)\sin\delta} \times (d\sin\beta + \cos\beta)\right] \times \left[1 - \frac{\cos\delta\sin\omega\sin\beta}{\cos(\phi-\beta)\cos\delta\cos\omega + \sin(\phi-\beta)\sin\delta} \times \left(\frac{d\sin\beta + \cos\beta}{l}\right)\right] \quad (18)$$

and $\xi \geq 0$ for non-negative values of both expressions in the parenthesis, otherwise, $\xi = 0$. It must be noted that ξ is dependent explicitly on d and l, while h is dependent explicitly on d only, but dependent implicitly on l through the hour angles ω_h and ω_s (see Appendix C). ω_h and ω_s are (in winter) the hour angles were the shadowing begins to climb or leave the collector, respectively.

Figures 9 and 10 describe h and ξ for vertical collectors ($\beta = 90°$) at different d, for January and $l = 7.5$, as a function of time. The curves are symetrical before noon. As d is increased, h and ξ change significantly. It can be seen that as $\omega \to \omega_{ss}$ (sunset), $h \to 1$ but ξ reaches a certain value. Figure 11 describes the changes of the shadow caused by a collector CL during the afternoon. Up to $\tau_h(\omega_h)$, the entire shadow is on the floor and at this instant it starts to touch the opposite collector MN. From that time on, the shadow is partly on the floor and partly on the MN collector. The shaded rectangle corresponds to time 16:30. At sunset, the shadow covers the whole collector height. The relative shaded area is about 0.41 (Fig. 10).

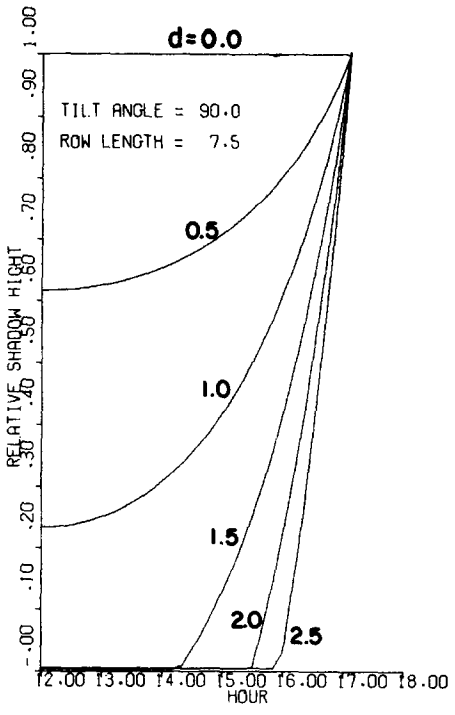

Fig. 9. Shadow height of a vertical collector.

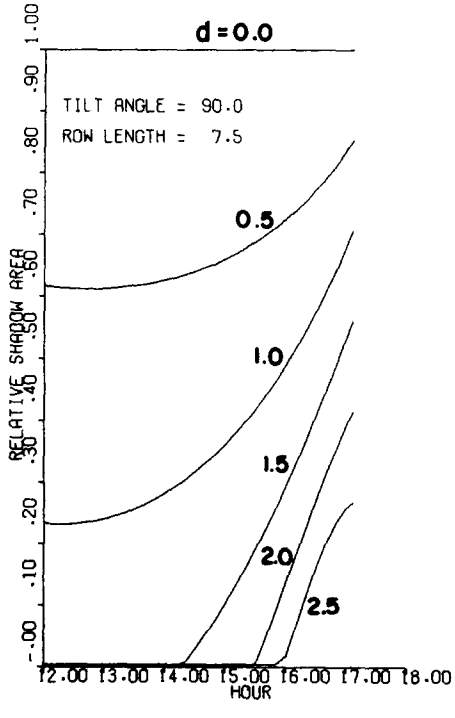

Fig. 10. Shadow area variation of a vertical collector.

Figure 12 describes the relative shaded area ξ for $\beta = 50°$ during a day in January for the arrangement shown in Fig. 7. The figure includes also the direct solar radiation falling on the inclined collector. The inflation of ξ curves (at the maximum shaded area) is explained by a faster decrease (with time) of the shadow length and a

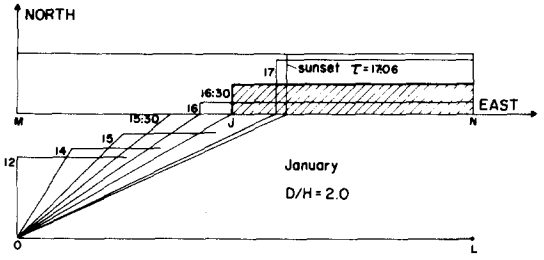

Fig. 11. Shadow variation of a vertical collector.

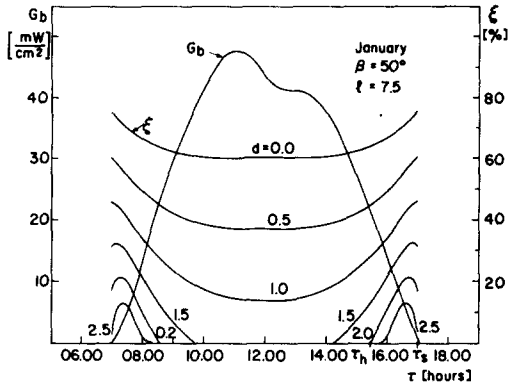

Fig. 12. Shadow area variation of an inclined collector.

slower increase in the shadow height. An important conclusion can be deducted from the figure. There is a critical relative distance d_c beyond which the gain in energy is insignificant. In this figure, $d_c = 2.0$. It should be noted that although $\xi(2.0)$ reaches up to 0.21, the radiation at this time is low since the time is close to sunset.

Figures 13 and 14 shows the effect of increasing the collector row length on the shadow height h and area ξ. Figures 13(a) and (b) describes the relative shadow heights and area for different collector spacing d and for $l = 5.0$. For $d = 2.0$, as an example, the shadow leaves the collector at the time $\tau_s(\omega_s) = 16{:}40$ when its height is 0.63 (see Appendix C). Figures 14(a) and (b) show h and ξ, respectively for $l = 25.0$. The behaviour is similar to that of Fig. 13. The conclusion from Figs. 13 and 14 is that the row length l has little effect on the shadow height h and shadow area ξ, since the effect of the length is pronounced only close to sunset (sunrise) where the radiation is low anyway. Increasing the row length beyond about $l = 25$ does not affect the shadow change any more.

Very useful information in the design of solar collector field is the spacing value between collectors as explained in the Introduction. The next section deals with the calculation of the optimum number of collector rows in a given field and hence the appropriate collector spacing is thus determined. This calculation is based on local insolation data. The following paragraph attempts to estimate the recommended collector spacing, based on shading effect only, for different latitudes.

Appendix C deals with the determination of the times where the shadow starts to climb, τ_h, or to leave, τ_s, the

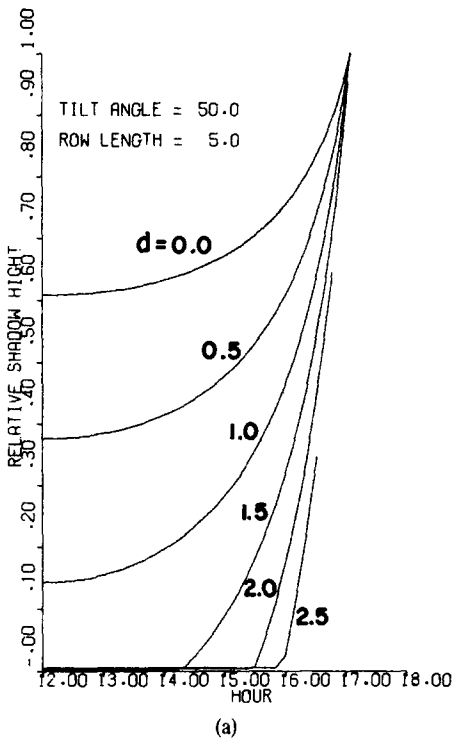

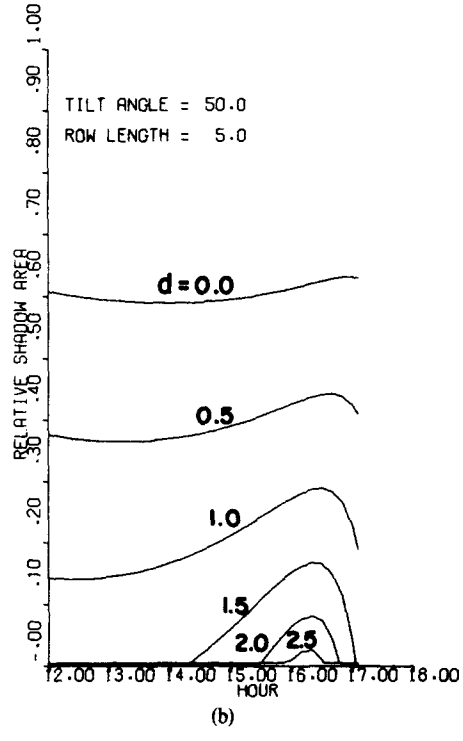

Fig. 13. Shadow (h and ξ) variation of an inclined collector, $l = 5.0$.

collector. The solar hour angle ω_h(eqn C4) for which the shadow starts to climb on the collector is independent of the tilt angle β and is strongly dependent on the collector spacing. τ_h is also independent of the row length l and is dependent on the collector location (latitude ϕ). Inspection of Figs. 9–14 reveals that for a certain collector

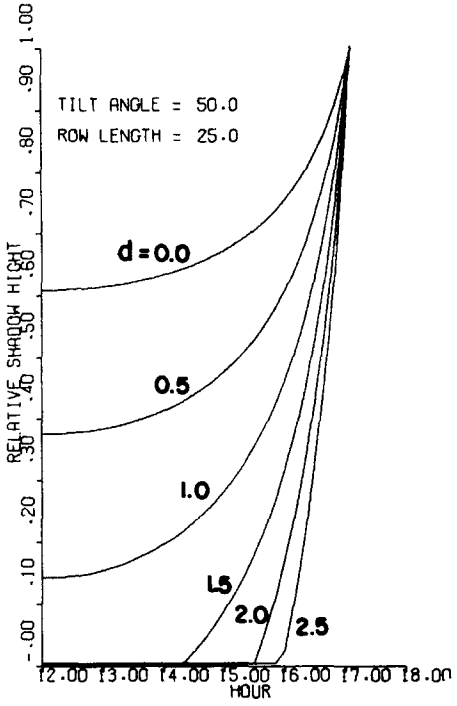

(a)

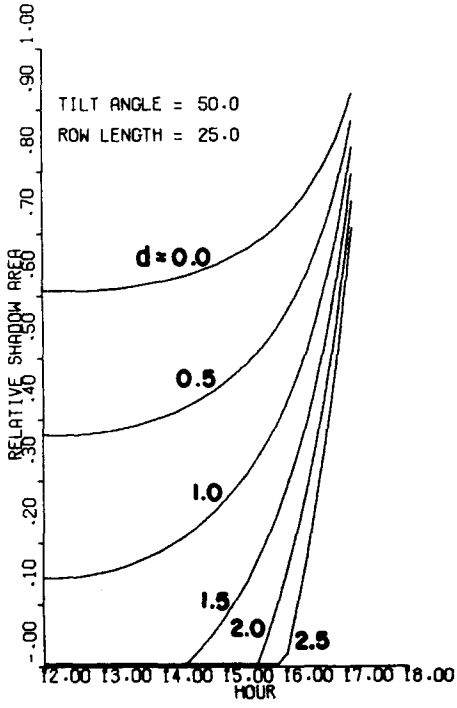

(b)

Fig. 14. Shadow (h and ξ) variation of an inclined collector, $l = 25.0$.

spacing (relative), d_c, and up the shadow occurs close to the sunset where the insolation is relatively low.

Figure 12 shows that the shading causes about 10 per cent decrease in collected radiation in a field of collectors spaced by $d_c = 2.0$ ($\phi = 32°$N). This calculation is obtained for the "worst case" (January), assuming that the collector is completely shaded from $\tau_h(d_c = 2.0) =$ 15:30 and on until sunset. The collector spacing for different latitudes might be obtained using the terms of τ_h and τ_{ss} in correct proportion to the case of $\phi = 32°N$ for which the deficiency of the 10 per cent of the collected energy was calculated. The determination of d_c by the above criteria becomes more valid for smaller l and β. Hence, the relative collector spacing d_c might be an estimate for the required collector spacing $D = \mathrm{d}H = \mathrm{d}A \sin \beta$. Table 2 contains recommended spacing, $\mathrm{d_c}$, for different latitudes.

Table 2. Recommended collector spacings

$\phi°N$	15	30	45	60
$\mathrm{d_c}$	1.3	2.0	3.7	11.0

SHADOW EFFECT ON THE COLLECTED ENERGY

The global short wave insolation composed by the direct and diffuse components is given by[5]

$$G = G_b \cos\theta + G_d \cos^2 \beta/2 \tag{19}$$

where G_b is the direct insolation on a surface perpendicular to the rays, G_d–diffuse insolation on a horizontal surface, θ–angle between the solar rays and the normal to the surface, and β–surface tilt angle. In eqn (19), the albedo and nearby surfaces reflection were neglected.

For a collector facing south, the relation between the different angles are[2, 5]

$$\cos\theta = \sin(\phi-\beta)\sin\delta + \cos(\phi-\beta)\cos\delta\cos\omega. \tag{20}$$

The total solar energy, (direct and diffuse), Q received by the collector, per unit area, in an average monthly day is

$$Q = \sum_j G_j \Delta\tau = \sum_j (G_{b_j}\cos\theta_j + G_{d_j}\cos^2\beta/2)\Delta\tau$$
$$= \sum_j G_{b_j}\cos\theta_j \Delta\tau + Q_d \cos^2\beta/2 \tag{21}$$

where the summation is on time from sunrise to sunset. In order to calculate Q, one needs the daily variation of the direct insolation G_{b_j} but needs only the total daily diffuse insolation Q_d.

A field of collectors arranged in rows is shown in Fig. 15. The assumption is that the first row is never shaded and all other rows might be shaded during the day by adjacent rows.

The direct insolation for a "shaded collector" is

$$G^s_{b_j} = AL(1-\xi_j)G_{b_j}\cos\theta_j \tag{22}$$

where ξ is given in eqn (18). Hence, the energy of direct radiation collected by a field of k rows is

$$Q_b{}^s = AL[\sum_j G_{b_j}\cos s\theta_j \Delta\tau + (k-1)\sum_j G_{b_j}(1-\xi_j)\cos\theta_j\Delta\tau]$$
$$k = 2, \ldots, k_m. \tag{23}$$

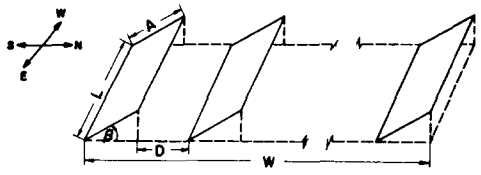

Fig. 15. A field of solar collectors.

The diffuse insolation collected by the field is effected by the geometry of the collector rows. Each row obscures part of the sky for the adjacent row. It is shown in Appendix B that the daily diffuse insolation received by a "shaded collector" is

$$G_d^s = G_d(\cos^2\beta/2 + \cos^2\eta_{av}/2 - 1). \tag{24}$$

Hence, the total daily solar energy received by a field of collectors of total area of kAL is

$$Q_t^s = AL\,[\sum_j G_{b_j}\cos\theta_j\Delta\tau + G_{d_j}\cos^2\beta/2 + (k-1)\sum_j(1-\xi_j)G_{b_j}\cos\theta_j\Delta\tau + (k-1)Q_d(\cos^2\beta/2 + \cos^2\eta_{av}/2 - 1)] \qquad k = 2,\ldots,k_m. \tag{25}$$

This energy is strongly dependent on the geometry of the collector. For different energy requirements and geometrical constraints of the field and collector, there exists an optimal deployment of the collectors in the given field.

Example

A field with dimensions LxW is to be installed with collectors facing south in rows of length L (Fig. 15). The collector width is A, its tilt angle β and the number of rows is $k(k = 2,\ldots,k_m)$. The trivial solution of one row inclined collector with area of $LW/\cos\beta$ is excluded because of limitation to the added height of $W\tan\beta$ and other structural and maintenance reasons. The spacing between rows are

$$D(k) = \frac{W - A\cos\beta}{k-1} - A\cos\beta \qquad k = 2,\ldots,k_m \tag{26}$$

where k_m is the maximum number of rows

$$k_m = \frac{W - A\cos\beta}{A\cos\beta + D_{\min}} + 1 \tag{27}$$

where $D_{\min}$ is the minimum spacing necessary for maintenance.

The present example refers to Tel-Aviv area (latitude 32°00'N, longitude 34° 49'E) with given insolation data[6] and available collector widths $A = 1, 2$ and 3 m. The field dimensions are $L = 7.5$ m, $W = 12$ m (90 m^2). The results are shown in Figs. 16 and 17 for January (the lowest solar insolation) using eqns (23) and (25) and performed with the aid of the computer.

Figure 16 describes the daily direct insolation energy collected by the receivers as a function of the number of rows k for different collector width A for two tilt angles $\beta = 30°$ (solid line) and $\beta = 60°$ (dashed line). For given k,

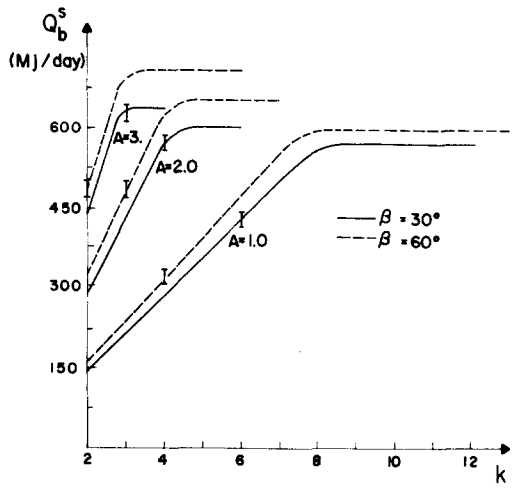

Fig. 16. Direct solar energy as a function of number of rows.

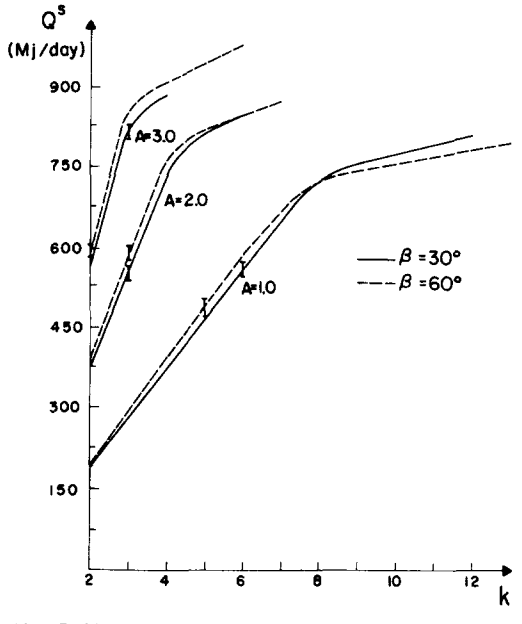

Fig. 17. Global solar energy as a function of number of rows.

β and A, the graphs indicate the daily energy. The spacing D is calculated from eqn (26). For $k = 2, \beta = 30°$ and $A = 1$ m, the daily collected energy is 144 MJ, the collector area is 15 m^2 and D = 10.27 m. By adding more rows, the energy increases until for 8 rows the curve starts to turn and the gain in energy with more collectors is no more significant. The number of rows for which shading starts to effect is marked by I on the curve. As the number of rows increases, the shading is more pronounced. The global solution (maximum energy received from minimum collector area) for this case is 8 rows with 60 m^2 which gives a daily energy of 558 MJ, and the spacing is $D = 0.72$ m. Higher energies are obtained for $\beta = 60°$ and bigger A. The curves are similar with an optimum number of rows (knee points). The over all optimal solution for the present example (Fig. 15) is $k = 3$, $A = 3$, $\beta = 60°$, $D = 3.75$, collector area 67.5 m^2 and

daily energy is 695 MJ. In this case, the row height is 2.6 m which might be too high.

In Fig. 17 the diffuse insolation was taken into account thus introducing the difference between this figure and Fig. 16. The curves do not bend sharply but still have the knee part where shading takes place and the contribution of the diffuse energy is more pronounced. There is no meaningful difference between $\beta = 30°$ and $\beta = 60°$. The optimal point for $A = 1$m and $\beta = 30°$ is 8 rows, $D =$ 0.72 m, collected area is 60 m^2 and the daily global energy is 724 MJ. The overall optimal solution for the present example is 3 rows $\beta = 50°$ (not shown in the figure), $D = 3.11$ m, total collector area 67.5 m^2 and the daily energy is 854 MJ.

CONCLUSIONS

The shadowing of collectors must be taken into account in large scale solar system design. "Real estate" field cost, limited available areas or the desire for compactness of the design from economical and energetical points of view may dictate a solution where shading is unavoidable. By increasing the number of rows for a given field (decreasing the spacing between collectors), the collectors area increases. On the other hand, this leads to a greater shading. Therefore an optimal solution exists for a required or maximal collected energy. The analysis in the example reveals that the collected energy reaches saturation for the direct insolation energy and increases slowly for the global energy. In this region shading takes place.

The optimal system design must involve the system cost, therefore maximum collected energy is only one part of the optimal solution. The other part is the average maximum collected energy per unit of collector area. The overall optimum solution would be the product of these two figures. The first part of the solution alone, (i.e. maximum energy) would lead to a large number of rows with a great shading effect. The second part of the solution suggests no shading effect, therefore the optimum number of rows is determined by the inflection point of the two components in the optimal solution where the effect of increase in energy is small with the increase in number of rows.

The system design parameters include insolation data, location (latitude), collector width A, tilt angle β, minimum spacing between collectors D_{min}, the field dimensions and the height of the collector above base. Each parameter contributes differently to the optimal solution (for example, the spacing d effects the solution strongly, whereas the row length l has only a small effect); the effect of some of them are shown in Figs. 16 and 17. In addition to the design parameters, the objective function (the system function to be optimized) has a great effect on the design. It should be noted that a total optimum system design solution was not fully analysed in this paper and is left for another study. A general and important result must be mentioned. For every latitude there is a critical spacing d_c, where for $d > d_c$ the shadow effect is insignificant. Table 2 presents the estimated critical spacing for latitudes 15°, 30°, 45° and 60° N. In the example, the optimal solution was obtained for $d \simeq 1.5$. The paper introduces an analysis of collector shadowing (its components, height and area) and its effect in the design of large solar systems.

Acknowledgement—The authors would like to thank the Ministry of Energy and infrastructure for their support in the study contract No. 78-1-41.

NOMENCLATURE

- A pole length (collector width)
- D collectors spacing
- d D/H
- F shadow length of a vertical pole
- G Global insolation
- G_b direct insolation
- G_d diffuse insolation
- H pole (collector) height
- H_s shadow height
- h H_s/A
- k row number
- L collector length
- l L/H
- P shadow length of an inclined pole
- Q energy
- W field width
- β tilt angle
- γ solar azimuth
- δ solar declination angle
- ξ relative shaded area of a collector
- η screening angle
- θ angle between the solar ray and the normal to the surface
- τ solar time
- ϕ latitude
- ω solar hour angle
- ω_{ss} sun set hour angle

REFERENCES

1. O. Barra, *et al.* Shadows' effect in a large scale solar power plant. *Solar Energy* **19**, 759–762 (1977).
2. N. Robinson, *Solar Radiation. Elsevier*, New-York, (1966).
3. J. I. Yellott, *Solar Energy Utilization for Heating and Cooling.* U. S. Government Printing Office (1976).
4. E. Coffari, A Mathematical Model for the Digital Computation of the Hours of Sunshine on an Inclined Plane. *Cooperation Mediterranee Pour L'energie Solaire* (Comples), pp. 10–15 (1976).
5. B. J. Gernier and A. Ohmura, The evaluation of surface variations in solar radiation income. *Solar Energy* **13**, 21–34 (1970).
6. A. Manes, A. Teitelman and J. Frilling, *Solar and Net Radiation.* Israel Meteorological Service, Bet-Dagan (1970).

APPENDIX A

A pole of length A (Fig. 18) in the ZY plane, inclined at angle β, causes a shadow on an inclined collector $MM'NN'$ placed at distance $OM = R$. The collector is perpendicular to the ZY plane and is inclined with respect to XY plane by the angle μ. The pole shadow components on the XY plane are $IC = P_X$ and $OI = P_Y$, and its shadow on the collector is EG. The coordinates of point E will now be calculated. This point is determined from the intersection of three planes $MM'NN'$, BCO' and OCO', where their equations are respectively

$$Z = (Y - R)\tan\mu \tag{A1}$$

$$X = P_X(Y - A\cos\beta)/(P_Y - A\cos\beta) \tag{A2}$$

$$Z = [(1 - P_Y/P_X)X + Y]\tan\beta \tag{A3}$$

The point E coordinates are obtained by solving the above equations

$$Z_E = A\sin\beta\frac{P_Y - R}{P_Y - A\cos\beta + (A\sin\beta/\tan\mu)} \tag{A4}$$

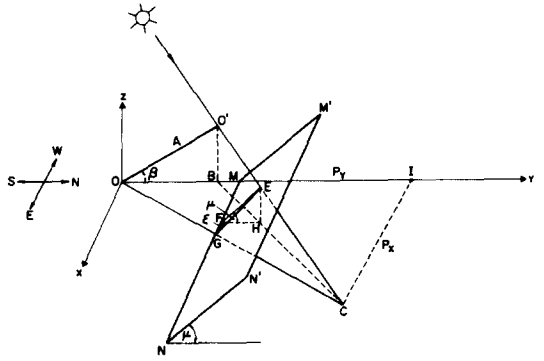

Fig. 18. The shadow of an inclined pole (at angle β) on an inclined collector (at angle μ).

$$Y_E = R + (Z_E/\tan\mu) \tag{A5}$$

$$X_E = [P_X/(P_Y - A\cos\beta)][(Z_E/\tan\mu) + R - A\cos\beta]. \tag{A6}$$

P_X and P_Y are given in eqns (11) and (12). From the geometry we obtain $MG = RP_X/P_Y$, $FG = MG - MF = (RP_X/P_Y) - X_E$, and

$$EF = EH/\sin\mu = Z_E/\sin\mu \tag{A7}$$

hence the angle ε between the shadow EG and the collector line MN is

$$\tan\epsilon = EF/FG = (Z_E/\sin\mu)/\left(\frac{P_X R}{P_Y} - X_E\right) \tag{A8}$$

The point G coordinates are $X_G = RP_X/P_Y$, $Y_G = R$, $Z_G = 0$ and the shadow line equation is

$$(X - X_G)/(X_E - X_G) = (Y - Y_G)/(Y_E - Y_G) = (Z - Z_G)/(Z_E - Z_G). \tag{A9}$$

For $\mu = \beta$, the coordinates of point E are

$$Z_E = (A\sin\beta/P_Y)(P_Y - R) \tag{A10}$$

$$Y_E = (A\cos\beta/P_Y)(P_Y - R) + R \tag{A11}$$

$$X_E = RP_X/P_Y. \tag{A12}$$

By substituting eqn (A12) into eqn (A8) we obtain $\varepsilon = 90°$, i.e. the pole shadow on the inclined collector is parallel to the pole ($EF = EG$). The shadow height is therefore (eqn (A7))

$$H_s = EF = A(1 - R/P_Y) \tag{A13}$$

The distance MF is given by eqn (A12)

$$g = X_E = RP_X/P_Y \tag{A14}$$

Let the pole represent the western edge of a similar $MM'NN'$ collector, then the relative shaded area on $MM'NN'$ is

$$\xi = \frac{H_s(L-g)}{AL} = (1 - R/P_Y)(1 - P_X R/P_Y L) \tag{A15}$$

where $MN = L$. $\xi \geq 0$ for non-negative values of both expressions in the parenthesis, otherwise $\xi = 0$. Equation (A15) can be rewritten as

$$\xi = \frac{H_s}{A}\left(\frac{L-g}{L}\right) = h \cdot s \tag{A16}$$

where h and s are the relative shadow height and length, respectively.

APPENDIX B

The diffuse solar radiation G_{d_β} received on a collector with a tilt angle β is[2, 5]

$$G_{d_\beta} = G_d \cos^2\beta/2. \tag{B1}$$

This approximate equation is based on the radiation that arrives from the part of the sky seen by the collector. For collectors arranged in rows, an additional part of the sky is obscured by an adjacent collector (Fig. 19). This part will now be calculated approximately. For a collector of length L placed at distance D from its neighbour and for large L/D the diffuse radiation arriving from the sides may be neglected. An incremental area Ldx at distance X is obscured by a "screening angle"

$$\eta = \arctan\left[\frac{(A-x)\sin\beta}{D + x\cos\beta}\right] \tag{B2}$$

since each incremental area along A is obscured by a different angle, the average screening angle is obtained by

$$\eta_{av} = \frac{1}{A}\int_0^A \arctan\left[\frac{(A-x)\sin\beta}{D + x\cos\beta}\right] dx. \tag{B3}$$

The diffuse radiation that does not fall on the collector resulting from the screening angle is $G_d(1-\cos^2\eta_{av}/2)$, therefore the diffuse radiation received by a collector in a row is

$$G_{d_\eta} = G_d\cos^2\beta/2 - G_d(1 - \cos^2\eta_{av}/2)$$

or

$$G_{d_\eta} = G_d(\cos^2\beta/2 + \cos^2\eta_{av}/2 - 1). \tag{B4}$$

APPENDIX C

In order to calculate the solar energy falling on a collector in presence of shadowing, the starting time τ_h where the shadow starts to climb, and the time τ_s where the shadow starts to leave the collector, must be determined.

In winter, the shadow is in the northern direction, and it is minimal at noon and increases toward morning and evening, Fig. 2. Figure 20 is a top view of two adjacent collectors. Curve 1 of collector II is a possibility of the shadow trajectory of the left edge of collector I. The shadow starts to climb on collector II at solar hour angle ω_h and at sunset the shadow is OA on the floor and AB on collector II, $h = AB = 1$. The shadow will remain on the collector at sunset if

$$\tan\psi_{ss} \geq \frac{d + \cos\beta}{l}. \tag{C1}$$

If eqn (C1) is not fulfilled ($h < 1$), then trajectory 2 takes place. The shadow will leave the collector at hour angle ω_s and from that time on the shadow will be on the floor only until sunset.

In summer, the shadow is at maximum at noon, Fig. 2, in the northern direction, and decreases toward morning and evening. Figure 21 shows two cases of possible shadow trajectories. For curve 1, the shadow leaves the collector at the hour angle ω_h, and remains from then on the floor. At ω_h, the east-west shadow

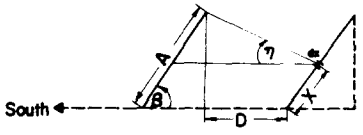

Fig. 19. The "screening angle" η.

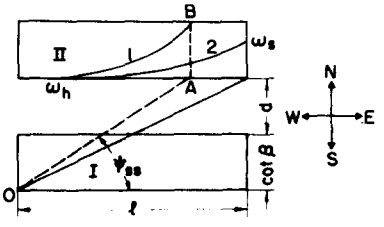

Fig. 20. Possible shadow trajectories in Winter.

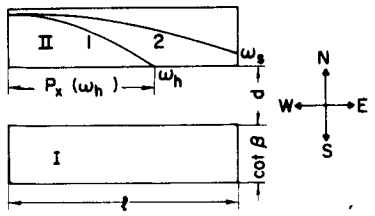

Fig. 21. Possible shadow trajectories in Summer.

component is not larger than the row length, i.e.

$$P_X(\omega_h) \leq l. \tag{C2}$$

If eqn (C2) is not fulfilled, then trajectory 2 takes place, ($h > 0$). The shadow leaves the collector at ω_s and from then on it will move on the floor. The determination of ω_h and ω_s will be derived from eqns (17) and (18) and (A16)

$$\xi = h \cdot s \tag{C3}$$

ξ might vanish for two cases:

(a) $s \neq 0, \quad h = 0$

$$h = 1 - \frac{\cos\phi \cos\delta \cos\omega + \sin\phi \sin\delta}{\cos(\phi - \beta)\cos\delta\cos\omega + \sin(\phi - \beta)\sin\delta} \times (d \sin\beta + \cos\beta) = 0$$

or

$$\omega_h(h = 0) = \arccos\left(\frac{\cos\phi + d\sin\phi}{\sin\phi - d\cos\phi}\tan\delta\right) \tag{C4}$$

(b) $h \neq 0, \quad s = 0$

$$s = 1 - \frac{\cos\delta \sin\omega}{\cos(\phi - \beta)\cos\delta\cos\omega + \sin(\phi - \beta)\sin\delta} \times \left(\frac{d\sin\beta + \cos\beta}{l}\right) = 0$$

and after some manipulations we obtain

$$[\cos\delta\,(d\sin\beta + \cos\beta)]\sin\omega - [l\cos(\phi - \beta)\cos\delta]\cos\omega - l\sin(\phi - \beta)\sin\delta = 0.$$

This equation is of the type

$$U\sin\omega + V\cos\omega + W = 0.$$

By setting $\omega = 2\Omega$[4] and using the trigonometric relations

$$\sin 2\Omega = 2\tan^2\Omega/(1 + \tan^2\Omega),$$

$$\cos 2\Omega = (1 - \tan^2\Omega)/(1 + \tan^2\Omega)$$

we get the quadratic equation for $\tan\Omega$

$$(W - V)\tan^2\Omega + 2U\tan\Omega + (W + V) = 0$$

the solution of which is

$$\omega_s(s = 0) = 2\arctan\left(\frac{-U \pm \sqrt{U^2 + V^2 - W^2}}{W - V}\right). \tag{C5}$$